Biomolecular simulations of membranes: Physical properties from different force fields

Shirley W. I. Siu[*] Robert Vacha [†] Pavel Jungwirth[†] Rainer A. Böckmann[*‡]

10.10.2007

Abstract

Phospholipid force fields are of ample importance for the simulation of artificial bilayers, membranes, and also for the simulation of integral membrane proteins. Here, we compare the two most applied atomic force fields for phospholipids, the all-atom CHARMM27 and the united atom Berger force field, with a newly developed all-atom generalized Amber force field (GAFF) for dioleoylphosphatidylcholine (DOPC) molecules. Only the latter displays the experimentally observed difference in the order of the C2 atom between the two acyl chains. The interfacial water dynamics is smoothly increased between the lipid carbonyl region and the bulk water phase for all force fields, however, the water order and with it the eletrostatic potential across the bilayer showed distinct differences between the force fields. Both Berger and GAFF underestimate the lipid self-diffusion. GAFF offers a consistent force field for the atomic scale simulation of biomembranes.

Key words: lipid force field; molecular dynamics simulation; AMBER; CHARMM; Berger; DOPC

[*]Address: Theoretical & Computational Membrane Biology, Center for Bioinformatics, Saarland University, P.O. Box 15 11 50, 66041 Saarbrücken, Germany

[†]Address: Institute of Organic Chemistry and Biochemistry, Academy of Sciences of the Czech Republic, and Center for Biomolecules and Complex Molecular Systems, Flemingovo nam. 2, 16610 Prague 6, Czech Republic

[‡]Corresponding author (rainer@bioinformatik.uni-saarland.de)

Introduction

Membranes are an indispensible constituent of biological cells. Apart from its apparent role in compartmentalization, they provide a unique hydrophilic and hydrophobic platform for the adsorption or anchoring of proteins to the interface, or for transmembrane proteins interacting mainly with the hydrophobic core. Lipid bilayers provide a highly modulative environment interacting, presumably affecting and possibly also keeping control of the function of e.g. membrane ion channels and pores. The lipid-protein interaction is exerted both by hydrophobic interactions between the lipid acyl chains and the protein surface and by polar interactions at the lipid-water interface. Changes in the interaction profile may be attained by variations in the (local) membrane composition or that of the surrounding solvent, or by changes in the temperature or pressure. Thereby, also the characteristic lateral pressure profile across the membrane is modified which may induce a shift of conformational equilibria between different states of membrane proteins, e.g. between the open and closed states of membrane channels (1, 2). Molecules strongly interacting with membranes are e.g. cholesterol (3, 4), anesthetics (5, 6), or monovalent (7, 8) and divalent cations (9, 10). The latter bind tightly to the carbonyl oxygens of phospholipids and thereby increase the lipid packing density as well as modify the lipid headgroup orientation (8, 10). Only recently, the importance of membrane thermodynamics for the understanding of propagating nerve pulses (11) or of the macroscopic effect of general anesthetic action (12) has been stressed.

Molecular dynamics (MD) simulation has been proven to be a powerful tool for the study of structural and dynamical properties of lipid membranes in atomic detail (13–15). In recent years with the dramatic increase in computing power, membrane simulation has reached a before unprecedented time scale, allowing the study of processes such as membrane assembly, fusion, domain formation, and protein/peptide/DNA interactions to be simulated while attaining statistical significance. In MD simulations, the intra- and intermolecular interactions of the lipids (also with the environment) are represented by specific potential functions (known as force fields). Parameters of the force fields are optimized empirically to reproduce both *ab initio* data as well as experimental observables. It was shown recently that the quality of the force field (rather than other technical issues connected with the simulations such as the system size) is the crucial ingredient for obtaining reliable computational results in simulations of lipid bilayers (16).

There are two most commonly used lipid force fields nowadays. The all-atom model CHARMM27 (17), evolved from the old CHARMM22 (18), was optimized on the condensed phase properties of alkanes. Similary, the united atom model of Berger et al. (19) (treating aliphatic hydrogen atoms implicitly), based on the united-atom version of OPLS (20), was parameterized against pentadecane. Both models have been applied extensively in a variety of membrane and membrane-protein studies and proved to show fairly agreeable results. Often, the Berger force field is preferred due to the greatly reduced computational cost with respect to all-atom lipid force fields (21). Frequently, the united-atom force field for lipids is combined with the all-atom OPLS (22) force field for the simulation of protein-membrane systems instead of the more consistent CHARMM force field for both lipids and proteins. The combination of different force fields, however, is not straightforward and requires careful investigation (21).
The main focus in parametrizations and tests of the lipid force field is typically on the reproduction of experimentally accessible lipid bilayer properties like the electron density profile, the area per lipid, the lipid order parameters, or the thickness of the membrane. These are generally well reproduced, with a few exceptions like the measured difference in the order parameters of the C2 atoms between the two acyl chains (typically similar in the force fields) or a too low lipid headgroup hydration at low water content (16). Also protein-lipid interactions in combined Berger/GROMOS or Berger/OPLS lipid-protein simulations are possibly overestimated, resulting in drastic changes of lipid properties upon insertion of proteins (21, 23). This is a consequence of the lack of experimental data on protein-lipid interactions to be used in parametrizations.

Deviations from experiment were also observed for the partitioning of anesthetics in lipid membranes: Molecular dynamics simulations of the spontaneous insertion of 1-alkanols of varying chain lengths into phosphatidylcholine bilayers applying the united-atom Berger force field for the lipids and the GROMOS force field for the 1-alkanols resulted in satisfying partition coefficients for the long-chain 1-alkanols (24). However, for ethanol the partition coefficient was increased by a factor of $7-200$ with respect to experiment, depending on the force field chosen for ethanol (24, 25). Similar large ethanol partition coefficients were also obtained by consistently applying the CHARMM27 all-atom force field (26).

Recently, the general all-atom AMBER force field (GAFF) was developed (27). In contrast to CHARMM and the previous version of AMBER, it is designed to be a general purpose force field, allowing extension to arbitrary organic molecules while keeping consistency with the parameters and forms of the existing force field. In principle, GAFF can also be used in membrane simulations, and in fact, Jójárt and Martinek (28) reported a tens of nanosecond test on GAFF in POPC lipid bilayer simulations in various ensembles, which showed its potency in good agreement with experimental values. Thus, the GAFF force field is expected to open the lane towards a consistent all-atom force field for proteins, lipids, and other arbitrary organic molecules.

Here, we developed an all-atom GAFF force field for DOPC combined with RESP (29, 30) atomic partial charges. In a first step, structural and dynamical properties of a fully hydrated DOPC bilayer were compared with those obtained applying the united atom force field of Berger et al. and with the all-atom CHARMM27 force field. Besides the structural and dynamical properties of the lipid bilayer, special emphasis was put on water properties close to the lipid-water interface and the resulting electrostatic potential across the phospholipid bilayer. Despite overall agreement in the reproduction of coarse properties of lipid bilayers, the force fields showed distinct differences in the phospholipid headgroup orientation, the water content of the interfacial region, the orientation of the carbonyl group, and the order of the two acyl chains. For the latter, only the GAFF force field reflected the experimentally found order asymmetry at the beginning of the chains.

Methods

Initial structures

Two different systems of dioleoylphosphatidylcholine (DOPC) bilayers were setup for this study: a full-atomistic model (with 72 DOPC lipids) for use with the general AMBER (GAFF) (27) and the CHARMM force fields (17), and a united-atom model (128 DOPC lipids) for use with the Berger force field (19).
A full-atomistic, pre-equilibrated DOPC bilayer (31)(1,500 ps snapshot, available from the web http://persweb.wabash.edu/facstaff/fellers) was taken as the starting structure. It consists of 72 lipids at a low hydration with only 5 – 6 water molecules per lipid. To ensure full hydration, the simulation box was enlarged and additional water molecules were added to the water phase to attain a water to lipid ratio of 37.9 (above the suggested experimental value (32) of 32.5). In total, the simulation system contained 2,727 water molecules, forming a water slab of about 1.8 nm thickness. The simulation system consists of 18,117 atoms.
The united-atom model was created from a pre-equilibrated POPC membrane model of 128 lipids (100 ns) used in our previous study (8). To convert to the DOPC model, the palmitoyl chain of each POPC lipid was modified to include two additional -CH2- groups in a *trans* conformation. The number of water molecules was 4,798 resulting in a water to lipid ratio of 37.4. The total system size was 21,279 atoms.

Force fields parameters

Three popular force fields were chosen in this study. The lipid parameters for the united atom model of DOPC were based on Berger. Parameters for the unsaturated carbons, however, were taken from the GROMOS87 force field (33). The CHARMM27 force field for DOPC was converted to GROMACS topology (conversion script kindly provided by Mark Abraham). Note that the conversion is not exact and dihedrals were fitted to Ryckaert-Bellemans dihedrals to reproduce the CHARMM27 (17) force field the best.
For GAFF, the atomic charges for the lipids were evaluated using antechamber with the restrained electrostatic potential fit method (RESP (29, 30)) after an *ab initio* HF/6-31G* calculation using the Gaussian03 program package (34) and fitting the electrostatic potential at points selected according to the Merz-Singh-Kollman scheme. The RESP fitted charges from 72 lipid conformations taken from the Feller model were averaged and rounded to two decimal points. The rounding was done with preference to conserve the total charge on a chemical group.
The total charges on the choline and phosphate groups, on the glycerol backbone, on the carbonyl groups and the acyl chains are similar for all investigated force fields. Differences are especially seen in the charge distribution of the choline group: the nitrogen atom is almost uncharged in the GAFF force field but highly negatively charged in the CHARMM27 and in the Berger force field (compare Table 1). The acyl chain atoms are neutral in the Berger force field, for GAFF only the beginning of the chain (C2 atom), the unsaturated carbons and the attached hydrogens as well as the terminal methyl groups carry charges significantly different from 0. In contrast, all atoms of the acyl chains have non-negligible charges in the CHARMM27 force field.

For the DOPC bilayer simulation applying the Berger force field the SPC water model (35) was chosen as this force field was developed with SPC water. For the same reason, the bilayer applying the CHARMM27 lipid force field was solvated with TIP3P water (36). For the newly developed GAFF force field, both the SPC/E (37) water model as well as the TIP3P water model (starting from a snapshot of the SPC/E system after 100 ns) were chosen for comparison.

Simulation conditions

All simulations were performed using the GROMACS package (38, 39). Periodic boundary conditions were applied in all directions. The system was coupled to a temperature bath at 310 K separately for the lipids and the water molecules with a coupling time constant of 0.1 ps^{-1} (40). Bonds to H-atoms were constrained using the LINCS (41) and the SETTLE algorithms (42). This allowed for an integration step size of 2 fs. The non-bonded pair list was updated every 10 steps with a cutoff of 1.0 nm. For the short range van der Waals interactions, a cutoff distance of 1.0 nm was used. In treating the long-range electrostatics, the Particle-Mesh Ewald (PME) method with a grid spacing of 0.12 nm and cubic interpolation was adopted.

Two systems were simulated in the *NPT* ensemble (GAFF all-atom and Berger united atom, systems A and E in Table 2), applying a semi-isotropic pressure coupling with a barostat relaxation time of 1 ps at a pressure of 1 bar (40). In order to ensure an area per lipid in agreement with experiment, DOPC bilayers simulated applying all-atom force fields were additionally subjected to a surface tension γ (*NP*γ*T* ensemble, $\gamma = 22$ dyns/cm per surface; systems B, C, D). The volume compressibility was chosen to 4.5×10^{-5} bar^{-1}. Data were collected every ps.

All simulation systems were energy minimized with the steepest descent method and subsequently simulated for 100 ns each. For the analyses, the first 20 ns were disregarded due to equilibration effects.

Table 2 gives a summary of the simulation systems presented in this manuscript. With a combination of different force fields, pressure coupling methods and water models, a total of five systems were studied and compared.

Analysis

Lipid order parameter

The lipid order parameter, S_{CD}, is a direct measurement of the acyl chain order or disorder from the quadrupolar splitting in the NMR experiment. For the simulations, the molecular order parameter is given by (13):

$$S_{ij} = \frac{1}{2}\langle 3cos\theta_i cos\theta_j - \delta_{ij}\rangle \quad (1)$$

where θ_i is the angle between the ith molecular axis ($i, j = x, y, z$) and the bilayer normal. When the C_nH bond vector is used as the molecular axis (say z), and about which the segment motion is assumed to be axially symmetric, then S_{zz} gives the experimentally measured S_{CD} value (43). For the united atom model which contains no explicit hydrogen atoms in the carbon tails, the segmental vector C_{n-1} to C_{n+1} is taken as the molecular axis of the C_n methylene group. The deuterium order parameter S_{CD} is approximated by the following relations for saturated and unsaturated carbon tail atoms (44)

$$-S_{CD}^{sat} = \frac{2}{3}S_{xx} + \frac{1}{3}S_{yy} \text{ and} \quad (2)$$

$$-S_{CD}^{unsat} = \frac{1}{4}S_{zz} + \frac{3}{4}S_{yy} \mp \frac{\sqrt{3}}{2}S_{yz}\ . \quad (3)$$

Lipid and water diffusion

The self-diffusion coefficient D of molecules can be calculated from the Einstein relation on Brownian motion:

$$2d_f D \quad = \quad \lim_{t\to\infty} \frac{1}{t} \langle (r(t) - r(0))^2 \rangle \tag{4}$$

d_f is the number of translational degrees of freedom (for lateral diffusion $d_f = 2$), and $r(t)$ the position of the molecule at time t. In practice, the lateral self-diffusion coefficient is estimated from the slope of the molecule's mean-square displacements d^2 (e.g. taken on the center of mass coordinates) in a defined time window averaged over all molecules N (45):

$$d^2(t) \quad = \quad \frac{1}{N} \frac{\Delta t}{T-t} \sum_{i=1}^{N} \sum_{t_0=0}^{T-t-1} |r(t_0) - r(t_0+t)|^2 \quad . \tag{5}$$

The first sum runs over the N molecules and the second sum runs over all time frames smaller than $T - t$, where T is the sampling time (Δt is the time between two subsequent conformations). For the lipids, the lateral mean-square displacements were corrected for the center of mass motion of the respective monolayer (45). The error was estimated by splitting the trajectories into pieces of 20 ns length (block averaging).
To obtain a spatially resolved water diffusion coefficient, the simulation box was divided into 40 slabs (i.e. ≈ 2 Å per slab) and the lateral diffusion in each slab was calculated by considering only the water molecules located in the same slab at time t_0 and at time $t_0 + t$. Block averaging from 5 ns pieces of the production trajectory was used to obtain the mean and standard error of the coefficients.
For comparison, additional simulations of pure water boxes (containing 2,182 water molecules, 5 ns simulation length each) yielded bulk water diffusion coefficients for the investigated water models.

Electrostatic potential

The electrostatic potential across the phospholipid bilayer was calculated by double integration of the averaged charge density ρ across the bilayer,

$$\phi(z) - \phi(z_\mathrm{o}) \quad = \quad -\frac{1}{\epsilon_\mathrm{o}} \int_{z_\mathrm{o}}^{z} dz' \int_{z_\mathrm{o}}^{z'} \rho(z'')dz'' \, . \tag{6}$$

Results

Area per lipid

The area per lipid is frequently used as a measure for the equilibration of the lipid bilayer system or to monitor phase transitions. In practice, the area per lipid is obtained as the lateral area of the simulation box (the xy-plane) divided by the number of lipids in one monolayer.
In Figure 2, the area per lipid for the 100 ns trajectory of each simulation system is presented. Equilibration in the area per lipid is reached after approximately 20 ns for each system, the analyses were conducted on the final 80 ns of the trajectories.
For a DOPC simulation appying the CHARMM27 force field without surface tension (data not shown) the area per lipid decreased to $0.56\,\mathrm{nm}^2$ within 16 ns. This transition to a gel-like state was previously observed for a DPPC bilayer applying the same force field in the *NPT* ensemble (46, 47). This transition can be prevented by application of a surface tension $\gamma = 22\,\mathrm{dyn/cm}$ (system D). Also for GAFF in the *NPT* ensemble the area per lipid was well below the crystallographic value ($0.62\,\mathrm{nm}^2$ vs. $0.72\,\mathrm{nm}^2$). Test simulations showed the best agreement to experimental data in the *NP*γ*T* ensemble by applying the same surface tension γ as for the CHARMM27 system (tested values $\gamma = 22, 30, 35\,\mathrm{dyn/cm}$).
Table 3 shows that the area per lipid agrees favorably with the experimental value of $72\,\mathrm{Å}^2$ for the GAFF and CHARMM27 systems (B, C, and D). However, lipids simulated in the Berger force field (*NPT*, system E) were too densely packed (area per lipid 8% below experiment).

Lipid headgroup orientation

Differences among the force fields in the lipid headgroup region are reflected e.g. in the headgroup tilt with respect to the bilayer normal. The headgroup tilt was taken as the angle between the vector connecting the phosphorus and the nitrogen atoms and the bilayer normal. The most probable orientations as well as the width of the distribution of tilt angles are summarized in Table 4. The largest lipid headgroup tilt angles were observed for the Berger force field (86°, system E) and the smallest for the GAFF force field (59° for system A, 67° for system B). The distribution of tilt angles is broad for all investigated force fields, with a width at half maximum of 62° (CHARMM27) to 88° (Berger). The difference in the lipid headgroup tilt is also reflected in the electron density profiles across the bilayer (see below). The straightened headgroup orientation in the CHARMM27 and in the GAFF force field enabled an increased water content in the interfacial membrane-water region.

Lipid order parameter

The ensemble averaged deuterium lipid order parameters $|\mathrm{S}_{CD}|$ of the two carbon tails are shown separately in Figure 3. All systems displayed the general trend of decreasing order along the chain towards the core of the bilayer with a prominent dip close to or at the double-bond segment (carbon atoms 9 and 10). Similar characteristics were observed for the oleoyl chain of POPC by deuterium NMR (48) and in molecular dynamics simulations (see e.g. the recent work by Pandit et al. (49)), and on DOPC by the DROSS NMR technique (50). Both ^{2}H-NMR and ^{1}H-^{13}C DROSS NMR found the dip located at the C10 atom.
In the MD simulations, however, the position of the central discontinuity differed among the investigated force fields: it occured in both chains at C9 for CHARMM27 (D), and at C10 for Berger (E), while for GAFF (B) the dip is seen at C11 for the *sn*-1 chain and at C10/C11 for the *sn*-2 chain (see Fig. 1 for the naming). Atoms more far away from the glycerol backbone (C12 – C18) showed the same order for both chains in all force fields, in agreement with NMR data. This finding was even observed for the saturated and unsaturated chains of POPC (48).
In contrast, deuterium NMR revealed differences close to the glycerol backbone even for identical chains: in studies on DPPC (51) and POPC (48) a distinctly smaller order was observed for the C2 atom of the *sn*-2 acyl chain as compared to the *sn*-1 chain. This inequivalence of the chains close to the glycerol backbone was found to be independent of the polar head group and thus to be a general feature of phospholipids within membranes (48). From NMR

results it was concluded that the initial orientations of the chains differ significantly with chain 1 being oriented perpendicular and chain 2 parallel to the bilayer surface (51). The suggestion of different conformations of the beginnings of the two chains was supported by X-ray diffraction studies (52). Only the new GAFF force field for DOPC reflected the general order characteristics with a significantly enhanced order for the C2 atom of the *sn*-1 chain. The Berger and CHARMM27 force fields show similar profiles for both chains close to the glycerol backbone as was also observed in earlier studies based on multi-nanosecond simulations (7, 24, 53). For DPPC, the C2 order for the *sn*-1 chain was even reported to be smaller than that of the *sn*-2 chain applying the CHARMM27 force field (17). A previous study on DOPC (54) applying a modified GROMOS96 force field (55) reported tiny differences for the C2 order parameters between the chains, together with the dip located at the C9 (54) atom similar to the CHARMM27 force field or at the C10 atom (55).

The initial chain conformation is described by the orientation of the vector connecting the C1 and the C2 atom: For both CHARMM27 and GAFF lipids, chain 1 is oriented perpendicular to the bilayer surface (maximum of the probability distribution of angles to bilayer normal $\approx 180^{\circ}$, data not shown). While the distribution is only slightly shifted to smaller angles for chain 2 in CHARMM27 (163°, width 44°), the second chain adopts a significantly different orientation with respect to chain 1 in the GAFF force field (133°, width 27°). Like for CHARMM27, the initial chain orientations for the Berger force field are similar with 160° and 144° for the two chains.

Density profile and membrane thickness

Electron density profiles of the simulated membrane systems can directly be compared to X-ray experimental data. Figure 4 shows the overall electron density and the electron densities of individual chemical groups of the bilayer.

The total electron density of the GAFF system without surface tension (A) shows good agreement with the X-ray data in the hydrophobic core region. However, the membrane thickness measured as the distance between the maxima of the electron denisty profiles is increased by $\approx 3\,$Å with respect to experiment (see Table 3). The GAFF-SPC/E system applying surface tension (B) revealed overall excellent agreement with the experimental profile. Using the TIP3P instead of the SPC/E water model together with GAFF (C) resulted in a decreased density at the membrane-water interface.
Also the electron density profile obtained for the CHARMM27 system (D) agrees well with the experimental profile, except for the region of the central methyl groups for which the density is significantly enhanced with respect to experiment. Due to the usage of the TIP3P water model the bulk water density is too small as is the case for the combination GAFF-TIP3P. Interestingly, systems with the TIP3P water model show enhanced bilayer fluctuations resulting in increased error bars for the membrane thickness (Table 3).
Although the membrane thickness is best modeled by the Berger force field (E), the electron density profile is at variance with the X-ray data. The headgroup region is broadened and the methyl group region is underestimated.

For comparion between the investigated force fields, Figure 5 shows a close-up view of the membrane-water interface for the GAFF-SPC/E, CHARMM27-TIP3P, and Berger-SPC force field combinations. Although the membrane thickness is similar for all three force fields, both CHARMM27 and GAFF show a drastically increased water content (*blue* lines) in the lipid headgroup region as compared to Berger, coupled to a decreased DOPC electron density (*red* lines). Also the carbonyl groups are shifted for Berger-SPC by $\approx 2\,$Å towards the headgroup region. The hydration of the carbonyl oxygens is significantly lowered for Berger lipids with respect to CHARMM27 and GAFF: The cumulative radial distribution yielded an average of only 1.5 water molecules around both carbonyl oxygens for Berger (taken at the first minimum of the radial distribution function, 0.55 for the *sn*-1 chain), but 3.4 (1.7) and 2.9 (1.4) water

molecules for CHARMM27 and GAFF lipids, respectively.

Lipid and water diffusion

Lipids in the liquid crystalline phase diffuse in the plane of the bilayer due to thermal agitation. This diffusive movement can be roughly classified into two regimes: fast fluctuation of the lipid in the local solvation cage (56) and a relatively slow but long distance diffusion in the bilayer. Different experimental methods acting on different time scales therefore obtain lipid diffusion coefficients differing by 2-3 orders of magnitude.

As shown in Figure 6 (upper panel) the lipid mean square displacement for all systems clearly showed the existence of both long-range and short-range diffusion behavior of lipids, with a smooth transition between both regions. In order to determine the linear segment in the mean square displacement curve (long-range diffusion), the diffusion coefficient D was calculated using different time windows for the linear fit.
The values for D (Fig. 6, lower panel) converged between 3 ns (for systems A, B, and E) and 5 ns (C and D). Therefore, the diffusion coefficients for long-range lipid diffusion were consistently computed from a linear fit to the mean square displacement between $5-10$ ns. The data are summarized in Table 5. With the exception of the bilayer simulated applying the CHARMM27 force field (system D), all computed diffusion coefficients are smaller by a factor of 2 to 8 as compared to the experimental value of $D = 13.7 \times 10^{-8}\,\mathrm{cm^2 s^{-1}}$ (NMR on oriented bilayers at 308 K (57)). Interestingly, the DOPC diffusion is strongly dependent also on the force field used for the water molecules: While GAFF combined with SPC/E water yields a lipid diffusion coefficient of $D = 3.1 \pm 0.9 \times 10^{-8}\,\mathrm{cm^2 s^{-1}}$, the diffusion is enhanced almost by a factor of 2 for GAFF combined with TIP3P water. Thus the increased bulk water diffusion of TIP3P with respect to SPC/E (see below) has a pronounced influence also on the lipids in a bilayer. Although the area per lipid is similar for both systems, the long-range lipid diffusion is about two times larger for the CHARMM27-TIP3P system as compared to GAFF-TIP3P. The CHARMM27 diffusion coefficient is, however, subject to a large error.
The diffusion coefficients obtained on the sub-nanosecond time scale decayed exponentially with increasing time scale. Values for the diffusion coefficient range between 5 and 82×10^{-8} $\mathrm{cm^2 s^{-1}}$, depending on the time scale and on the applied force field, and are in agreement with experimental diffusion coefficients obtained for DPPC of $10-100 \times 10^{-8}\,\mathrm{cm^2 s^{-1}}$ (56, 58, 59).

The (lateral) water diffusion close to the phospholipid bilayer and in the interfacial region depends strongly on the water model applied in the simulation (see Fig. 7). While SPC/E water in GAFF simulations was largely immobilized in the interfacial region (*blue* and *black lines*, see also Lopez et al. (60)), both Berger-SPC and CHARMM27-TIP3P resulted in a comparingly large water diffusion of $1 - 3 \times 10^{-5}\,\mathrm{cm^2/s}$. This is at least partially caused by the enhanced bulk diffusion values for these water models (61) as compared to experiment ($2.92 \times 10^{-5}\,\mathrm{cm^2/s}$ at 35°C, see Mills (62)).

Electrostatic potential and dipole moment

The total electrostatic potential across the lipid bilayer showed similar features for the different investigated force fields (see Figure 8): the potential was positive inside the bilayer which is in agreement with previous simulation studies on PC membranes at sufficient hydration (see e.g. (8, 63, 64)) and experiments (65). The phospholipid headgroups contribute a negative potential (*solid* lines in Fig. 8, lower panel) which is overcompensated by the opposed water dipole orientation (*dashed* lines) in the interfacial region resulting in a total positive electrostatic potential. The orientation of water dipoles was found previously to be reduced in the presence of salt ions (8).
Both all-atom force fields have a distinct potential maximum at the bilayer center, caused by

the non-zero partial charges on the terminal methyl groups. While the total electrostatic potential for the CHARMM27 system rises first in the region of the carbonyl groups, the potential for the GAFF system steeply increases in the choline/phosphate region (similar for both investigated water models). For the latter, the potential decreases slightly towards the unsaturated carbons of the chains followed by the central maximum. The Berger force field showed a flat potential in the region of the hydrocarbon chains which is due to the uncharged hydrocarbon tail atoms.

Besides the PC headgroup, mainly the fatty acid carbonyl groups contribute to the molecular dipole moment (see also distribution of partial charges in Table 1). In crystal structures at very low hydration (2 water molecules per lipid) an asymmetry between the carbonyl orientations of the *sn*-1 and *sn*-2 was observed (66, 67). The *sn*-1 carbonyl oriented parallel to the bilayer plane and the *sn*-2 carbonyl was found in two different conformations, both pointing towards the water phase (partially negatively charged oxygen pointing out of the hydrophobic core).
All force fields showed broad gaussian-like distributions of C=O orientations with respect to the bilayer normal (data not shown). Within the Berger force field, the most probable angle ϕ between the C=O vector and the membrane normal was shifted from 60° to 31° between the *sn*-1 and *sn*-2 carbonyls, the probabilities of finding angles below 90° (carbonyl pointing to the water phase, carbonyl dipole towards hydrophobic core) are 86% and 97%, respectively. For GAFF (with surface tension, SPC/E water), an increase in ϕ from 54° to 69° was observed, the probability of finding a carbonyl pointing to the water phase is 93% for the *sn*-1 and 76% for the *sn*-2 carbonyl. The most probable carbonyl angles for the acyl chains in the CHARMM27 force field are 44° and 69°, however, the probabilities for angles $\leq 90^{\circ}$ were similar for both chains with 70%.

The water order in the interfacial region is further investigated in Fig. 9 showing the mean dipole moment of water molecules depending on their position relative to the lipid bilayer. Both Berger and GAFF systems revealed two regions of positive water dipole moment (pointing into the membrane, opposite to the lipid dipoles), one in the region of the choline and phosphate groups and the second at the hydrophobic interface close to the carbonyl groups. The water orientation is more pronounced for the Berger force field. This is due to the increased total dipole moment of Berger lipids ($\approx 15\%$ with respect to GAFF and CHAMM27) and the two times larger component of the dipole moment normal to the membrane (Table 4). For the CHARMM27 system (D), the water dipole orientation at the interface headgroup-hydrophobic core is reversed with respect to the other force fields. Both the water model (TIP3P) as well as the significant amount of carbonyl dipoles pointing into the hydrophobic core ($\approx$30%) for CHARMM27 are presumably the cause for this reversed water dipole orientation.

Discussion

All three investigated lipid force fields were shown to correctly describe the coarse properties of phospholipid bilayers. However, the two most frequently applied force fields, CHARMM27 and Berger, did not reproduce the experimentally found order parameter dependence of the C2 atom on the acyl chain, in contrast to the newly developed GAFF force field for DOPC molecules. Also the different initial orientations of the two chains with respect to the bilayer normal appear to be best described by the GAFF force field. Interestingly, Jojart and Martinek (28) did not observe significant differences between the C2 atom orders of the palmitoyl and the oleyl chains of POPC applying the GAFF force field. Order parameters reported for the recently developed GROMOS96 45A3 force field for phospholipids (68) also show an enhanced order for the C2 atom of the *sn*-1 chain (DPPC). However, the latter two studies were probably based on too short sampling times (4 ns and 300 ps, respectively). A recent reparametrization of the partial charges in the CHARMM27 force field enabling simulations of the fluid phase in the *NPT* ensemble (47) did not yield improved C2 atom orders with respect to the original CHARMM27.

Both structural and dynamical properties of the aqueous solution at the water-phospholipid bilayer interface (for a thorough review on this topic see Berkowitz et al. (15)) were shown to depend on the phospholipid force field: The ordering of water molecules within the lipid-water interface depends crucially on the chosen lipid force field. For CHARMM27, the total electrostatic potential was shown to rise first in the region of the carbonyl groups. Together with the experimental finding that removal of the carbonyl groups only partly accounts for the positive electrostatic potential inside lipid bilayers (65) this may question the applicability of the CHARMM27 force field in cases where the potential is crucial to e.g. the structure or function of membrane-associated proteins or in the electrostatically driven binding of molecules to membranes.

Also the water dynamics close to membrane interface is crucially dependent on the applied force field: CHARMM27 was developed applying the TIP3P water model, the Berger force field together with SPC water, and GAFF may be used with both TIP3P and with SPC/E. Only the SPC/E water correctly reflects the bulk water diffusion coefficient, TIP3P overestimates the bulk water diffusion by more than a factor of 2. For the CHARMM27 lipid bilayer simulation, the used 38 water molecules per lipid were not sufficient to reach full hydration, since the water diffusion between periodic bilayers did not reach the increased bulk water diffusion for the TIP3P water model. In contrast, for SPC and SPC/E water this hydration level was sufficient to reach the bulk water diffusion. The lateral diffusion coefficient for lipids is too small for the GAFF and Berger force fields applying the SPC(/E) water models. In contrast, the CHARMM27 lipid force field shows a diffusion close to the experimental value. One possible reason may be due to the noteworthy charges on the acyl chain atoms in the CHARMM27 force field. However, the diffusion is partly enhanced also due to the large diffusion coefficient for water molecules applying the TIP3P model.

Summary

In the present study we show simulation results for a DOPC membrane employing a newly developed all atom force field based on GAFF. The performance of this force field against two existing parametrizations (the all atom CHARMM27 and the united atom model by Berger) is tested on a range of physical observables. The presented GAFF force field reproduces both the coarse properties like the bilayer thickness, but also the experimentally found differences in the structure and the order of the two acyl chains. In addition, GAFF offers a consistent force field for both lipids and membrane embedded proteins, thereby enabling detailed studies of the interaction between lipids and proteins. It has been argued that the *NPT* ensemble is appropriate for lipid bilayer simulations (19, 69). Both GAFF and CHARMM27 lipid force

fields showed a transition to a gel-like state in this ensemble, making the use of a surface tension mandatory in simulations of the fluid (L_α) phase. In case of CHARMM27, a reparametrizations of the partial atomic charges has been shown to pave the way towards fluid phase simulations in the *NPT* ensemble for DPPC (47). One possible reason for deviations from the fluid-like behaviour of bilayers simulated in the *NPT* ensemble may be the neglect of polarizability. Especially the large fields occuring at the interface between the highly polar water phase and the low-dielectric hydrocarbon interior underline the need for a careful investigation of polarization effects. To this end, development and tests of a polarizable model are currently under way.
Apart from the polarization issue, future studies will focus on the lipid-protein interaction in the different force fields. However, comparison to experimental data is currently limited due to the scarcity of detailed experimental studies on these interactions. Since GAFF easily allows extension to arbitrary organic molecules it can also be applied to systematic studies on the partitioning of solutes between the solvent and the bilayer, of great importance for a more thorough understanding of dose – response relationships in medicine. Knowledge about the binding characteristics may additionally prove useful for future drug development.

Acknowledgements

We thank Volkhard Helms for support with computing time and Beate Griepernau for help with the analysis. We thank Mark Abraham for providing the script for the conversion of the CHARMM27 force field to Gromacs, and for a lot of helpful discussions about its use. Financial support by the Deutsche Forschungsgemeinschaft (Graduate School *Structure Formation and Transport in Complex Systems*, No. 1276/1) is acknowledged. As members of the Center for Bioinformatics, Rainer A. Böckmann and Shirley Siu are supported by the Deutsche Forschungsgemeinschaft Grant BIZ 4/1. Robert Vacha and Pavel Jungwirth thank the Grant Agency of the Academy of Sciences (Grant No. A400400503) and the Czech Ministry of Education (Grant No. LC512). R.V. acknowledges support from the Granting Agency of the Czech Republic (grant 203/05/H001).

PDB files of equilibrated snapshots, and the GROMACS implementations of the used Berger and CHARMM27 force field as well as that of the developed GAFF force field for DOPC molecules are available free of charge on the websites http://www.bioinf.uni-sb.de/RB and http://www.molecular.cz/∼vacha/downloade.htm.

References

1. Trudell, J. R., 1977. A unitary theory of anesthesia based on lateral phase separations in nerve membranes. *Anesthesiology* 46:5–10.

2. Cantor, R. S., 1997. The Lateral Pressure Profile in Membranes: A Physical Mechanism of General Anesthesia. *Biochemistry* 36:2339–2344.

3. Silvius, J. R., 2003. Role of cholesterol in lipid raft formation: lessons from lipid model systems. *Biochim. Biophys. Acta* 1610:174–183.

4. Hofsäß, C., E. Lindahl, and O. Edholm, 2003. Molecular dynamics simulations of phospholipid bilayers with cholesterol. *Biophys. J.* 84:2192–2206.

5. Urban, B. W., 2006. Interactions of anesthetics with their targets: Non-specific, specific or both? *Pharmacology & Therapeutics* 111:729–770.

6. Högberg, C.-J., and A. P. Lyubartsev, 2007. Effect of local anesthetic lidocaine on electrostatic properties of a lipid bilayer. *Biophys. J.* doi:10.1529/biophysj.107.104208.

7. Pandit, S. A., D. Bostick, and M. L. Berkowitz, 2003. Molecular Dynamics Simulation of a Dipalmitoylphosphatidylcholine Bilayer with NaCl. *Biophys. J.* 84:3743–3750.

8. Böckmann, R. A., A. Hac, T. Heimburg, and H. Grubmüller, 2003. Effect of Sodium Chloride on a Lipid Bilayer. *Biophys. J.* 85:1647–1655.

9. L. Herbette, C. A. N., and R. V. McDaniel, 1984. Direct Determination of the Calcium profile Structure for Dipalmitoyllecithin Multilayers Using Neutron Diffraction. *Biophys. J.* 46:677–685.

10. Böckmann, R. A., and H. Grubmüller, 2004. Multistep binding of divalent cations to phospholipid bilayers: A molecular dynamics study. *Angew. Chem. Int. Ed. Engl.* 43:1021–1024.

11. Heimburg, T., and A. D. Jackson, 2005. On soliton propagation in biomembranes and nerves. *Proc. Natl. Acad. Sci. USA* 102:9790–9795.

12. Heimburg, T., and A. D. Jackson, 2007. The thermodynamics of general anesthesia. *Biophys. J.* 92:3159–3165.

13. Tieleman, D. P., S. J. Marrink, and H. J. C. Berendsen, 1997. A Computer Perspective of Membranes: Molecular Dynamics Studies of Lipid Bilayer Systems. *Biochim. Biophys. Acta* 1331:235–270.

14. Ash, W. L., M. R. Zlomislic, E. O. Oloo, and D. P. Tieleman, 2004. Computer simulations of membrane proteins. *Biochim. Biophys. Acta* 1666:158–189.

15. Berkowitz, M. L., D. L. Bostick, and S. Pandit, 2006. Aqueous solutions next to phospholipid membrane surfaces: Insights from simulations. *Chem. Rev.* 106:1527–1539.

16. Castro-Roman, F., R. W. Benz, S. H. White, and D. J. Tobias, 2006. Investigation of finite-system-size effects in molecular dynamics simulations of lipid bilayers. *J. Phys. Chem. B* 110:24157–24164.

17. Feller, S. E., and J. A. D. MacKerell, 2000. An improved empiricial potential energy function for molecular simulations of phospholipids. *J. Phys. Chem. B* 104:7510–7515.

18. Schlenkrich, M., J. Brickmann, A. D. MacKerell, and M. Karplus, 1996. Empirical potential energy function for phospholipids: Criteria for parameter optimization and applications., Birkhäuser, 31–81.

19. Berger, O., O. Edholm, and F. Jähnig, 1997. Molecular dynamics simulations of a fluid bilayer of dipalmitoylphosphatidylcholine at full hydration, constant pressure, and constant temperature. *Biophys. J.* 72:2002–2013.

20. Jorgensen, W. L., and J. Tirado-Rives, 1988. The OPLS potential functions for proteins. Energy minimizations for crystals of cyclic peptides and crambin. *J. Am. Chem. Soc.* 110:1657–1666.

21. Tieleman, D. P., J. L. MacCallum, W. L. Ash, C. Kandt, Z. Xu, and L. Monticelli, 2006. Membrane protein simulations with a united-atom lipid and all-atom protein model: lipid-protein interactions, side chain transfer free energies and model proteins. *J. Phys.: Condens. Matter* 18:S1221–S1234.

22. Kaminski, G., R. A. Friesner, J. Tirado-Rives, and W. L. Jorgensen, 2001. Evaluation and Reparametrization of the OPLS-AA Force Field for Proteins via Comparison with Accurate Quantum Chemical Calculations on Peptides. *J. Phys. Chem. B* 105:6474–6487.

23. Siu, S. W. I., and R. A. Böckmann, 2007. Electric field effects on membranes: gramicidin A as a test ground. *J. Struct. Biol.* 157:545–556.

24. Griepernau, B., S. Leis, M. F. Schneider, M. Sikor, D. Steppich, and R. A. Böckmann, 2007. 1-Alkanols and Membranes: A Story of Attraction. *Biochim. Biophys. Acta* In press.

25. Patra, M., E. Salonen, E. Terama, I. Vattulainen, R. Faller, B. W. Lee, J. Holopainen, and M. Karttunen, 2006. Under the Influence of Alcohol: The Effect of Ethanol and Methanol on Lipid Bilayers. *Biophys. J.* 90:1121–1135.

26. Chanda, J., and S. Bandyopadhyay, 2006. Perturbation of Phospholipid Bilayer Properties by Ethanol at a High Concentration. *Langmuir* 22:3775–3781.

27. Wang, J., R. M. Wolf, J. W. Caldwell, P. A. Kollman, and D. A. Case, 2004. Development and testing of a general AMBER force field. *J. Comp. Chem.* 25:1157–1174.

28. Jójárt, B., and T. A. Martinek, 2007. Performance of the general Amber force field in modeling aqueous POPC membrane bilayers. *J. Comp. Chem.* 28:2051–2058.

29. Bayly, C. I., P. Cieplak, W. D. Cornell, and P. A. Kollman, 1993. A well-behaved electrostatic potential based method using charge restraints for deriving atomic charges: the RESP model. *J. Phys. Chem.* 97:10269–10280.

30. Cornell, W. D., P. Cieplak, C. I. Bayly, and P. A. Kollman, 1993. Application of RESP charges to calculate conformational energies, hydrogen bond energies, and free energies of solvation. *J. Am. Chem. Soc.* 115:9620–9631.

31. Feller, S. E., D. Yin, R. W. Pastor, and A. D. MacKerell, 1997. Molecular dynamics simulation of unsaturated lipid bilayers at low hydration: parameterization and comparison with diffraction studies. *Biophys. J.* 73:2269–2279.

32. Tristram-Nagle, S., H. I. Petrache, and J. F. Nagle, 1998. Structure and interations of fully hydrated dioleoylphosphatidylcholine bilayers. *Biophys. J.* 75:917–925.

33. Gunsteren, W. F. V., and H. J. C. Berendsen, 1987. Gromos User Manual. BIOMOS biomolecular software, Laboratory of Physical Chemistry, University of Groningen, The Netherlands.

34. Frisch, M. J., G. W. Trucks, H. B. Schlegel, G. E. Scuseria, M. A. Robb, J. R. Cheeseman, J. A. Montgomery, Jr., T. Vreven, K. N. Kudin, J. C. Burant, J. M. Millam, S. S. Iyengar, J. Tomasi, V. Barone, B. Mennucci, M. Cossi, G. Scalmani, N. Rega, G. A. Petersson, H. Nakatsuji, M. Hada, M. Ehara, K. Toyota, R. Fukuda, J. Hasegawa, M. Ishida, T. Nakajima, Y. Honda, O. Kitao, H. Nakai, M. Klene, X. Li, J. E. Knox, H. P. Hratchian, J. B. Cross, V. Bakken, C. Adamo, J. Jaramillo, R. Gomperts, R. E. Stratmann, O. Yazyev, A. J. Austin, R. Cammi, C. Pomelli, J. W. Ochterski, P. Y. Ayala, K. Morokuma, G. A. Voth, P. Salvador, J. J. Dannenberg, V. G. Zakrzewski, S. Dapprich, A. D. Daniels, M. C. Strain, O. Farkas, D. K. Malick, A. D. Rabuck, K. Raghavachari, J. B. Foresman, J. V. Ortiz, Q. Cui, A. G. Baboul, S. Clifford, J. Cioslowski, B. B. Stefanov, G. Liu, A. Liashenko, P. Piskorz, I. Komaromi, R. L. Martin, D. J. Fox, T. Keith, M. A. Al-Laham, C. Y. Peng, A. Nanayakkara, M. Challacombe, P. M. W. Gill, B. Johnson, W. Chen, M. W. Wong, C. Gonzalez, and J. A. Pople. Gaussian 03, Revision C.02. Gaussian, Inc., Wallingford, CT, 2004.

35. Berendsen, H. J. C., J. P. M. Postma, W. F. Van Gunsteren, and J. Hermans, 1981. Interaction model for water in relation to protein hydration., D. Reidel Publishing Company, Dordrecht, The Netherlands, 331–342.

36. Jorgensen, W. L., J. Chandrasekhar, and J. D. Madura, 1983. Comparison of simple potential functions for simulating liquid water. *J. Chem. Phys.* 79:926–935.

37. Berendsen, H. J. C., J. R. Grigera, and T. P. Straatsma, 1987. The missing term in effective pair potentials. *J. Phys. Chem.* 91:6269–6271.

38. Berendsen, H. J. C., D. van der Spoel, and R. van Drunen, 1995. GROMACS: A message-passing parallel molecular dynamics implementation. *Computer Phys. Comm.* 91:43–56.

39. Lindahl, E., B. Hess, and D. van der Spoel, 2001. GROMACS 3.0: A package for molecular simulation and trajectory analysis. *J. Mol. Model.* 7:306–317.

40. Berendsen, H. J. C., J. P. M. Postma, W. F. van Gunsteren, A. Dinola, and J. R. Haak, 1984. Molecular dynamics with coupling to an external bath. *J. Chem. Phys.* 81:3684–3690.

41. Hess, B., H. Bekker, H. J. C. Berendsen, and J. G. E. M. Fraaije, 1997. LINCS: A Linear Constraint Solver for molecular simulations. *J. Comp. Chem.* 18:1463–1472.

42. Miyamoto, S., and P. A. Kollman, 1992. SETTLE – an analytical version of the SHAKE and RATTLE algorithm for rigid water models. *J. Comp. Chem.* 13:952–962.

43. Seelig, J., 1977. Deuterium magnetic resonance: theory and application to lipid membranes. *Quarterly Reviews of Biophysics* 10:353–418.

44. Douliez, J. P., A. Ferrarini, and E. J. Dufourc, 1998. On the relationship between C-C and C-D order parameters and its use for studying the conformation of lipid acyl chains in biomembranes. *J. Chem. Phys.* 109:2513–2518.

45. Böckmann, R. A., A. Hac, T. Heimburg, and H. Grubmüller, 2003. Effect of Sodium Chloride on a Lipid Bilayer. *Biophys. J.* 85:1647–1655.

46. Jensen, M. O., O. G. Mouritsen, and G. H. Peters, 2004. Simulations of a Membrane-Anchored Peptide: Structure, Dynamics, and Influence on Bilayer Properties. *Biophys. J.* 86:3556–3575.

47. Sonne, J., M. O. Jensen, F. Y. Hansen, L. Hemmingsen, and G. H. Peters, 2007. Reparametrization of all-atom dipalmitoylphosphatidylcholine lipid parameters enables simulation of fluid bilayers at zero tension. *Biophys. J.* 92:4157–4167.

48. Seelig, J., and N. Waespe-Sarcevic, 1978. Molecular order in Cis and Trans unsaturated phospholipid bilayers. *Biochemistry* 17:3310–3315.

49. Pandit, S. A., S.-W. Chiu, E. Jakobsson, A. Grama, and H. L. Scott, 2007. Cholesterol surrogates: A comparison of Cholesterol and 16:0 Ceramide in POPC bilayers. *Biophys. J.* 92:920–927.

50. Warschawski, D. E., and P. F. Devaux, 2005. Order parameters of unsaturated phospholipids in membranes and the effect of cholesterol: a ^{1}H-^{1}3C solid-state NMR study at natural abundance. *Europ. Biophys. J.* 34:987–996.

51. Seelig, A., and J. Seelig, 1975. Bilayers of dipalmitoyl-3-*sn*-phosphatidylcholine – conformational differences between the fatty acyl chains. *Biochim. Biophys. Acta* 406:1–5.

52. Hitchcock, P. B., R. Mason, K. M. Thomas, and G. G. Shipley, 1974. Structural chemistry of 1,2 dilauroyl-DL-phosphatidylethanolamine: Molecular conformation and intermolecular packing of phospholipids. *Proc. Natl. Acad. Sci. USA* 71:3036–3040.

53. Klauda, J. B., B. R. Brooks, A. D. MacKerell, R. M. Venable, and R. W. Pastor, 2005. An ab initio study on the torsional surface of alkanes and its effect on molecular simulations of alkanes and a DPPC bilayer. *J. Phys. Chem. B* 109:5300–5311.

54. Bhide, S. Y., and M. L. Berkowitz, 2005. Structure and dynamics of water at the interface with phospholipid bilayers. *J. Chem. Phys.* 123:224702.

55. Chiu, S. W., E. Jakobsson, S. Subramaniam, and H. L. Scott, 1999. Combined Monte Carlo and molecular dynamics simulation of fully hydrated dioleyl and palmitoyl-oleyl phosphatidylcholine lipid bilayers. *Biophys. J.* 77:2462–2469.

56. König, S., T. M. Bayerl, G. Coddens, D. Richter, and E. Sackmann, 1995. Hydration dependence of chain dynamics and local diffusion in L-α-Dipalmitoylphosphtidylcholine multilayers studied by incoherent quasi-elastic neutron scattering. *Biophys. J.* 68:1871–1880.

57. Filippov, A., G. Orädd, and G. Lindblom, 2003. Influence of Cholesterol and water content on phospholipid lateral diffusion in bilayers. *Langmuir* 19:6397–6400.

58. Pfeiffer, W., T. Henkel, E. Sackmann, and W. Knoll, 1989. Local dynamics of lipid bilayers studied by incoherent quasi-elastic neutron scattering. *Europhys. Lett.* 8:201–206.

59. Tabony, J., and B. Perly, 1990. Quasielastic neutron scattering measurements of fast local translational diffusion of lipid molecules in phospholipid bilayers. *Biochim. Biophys. Acta* 1063:67–72.

60. Lopez, C. F., S. O. Nielsen, and M. L. Klein, 2004. Hydrogen bonding structure and dynamics of water at the dimyristoylphosphatidylcholine lipid bilayer surface from a molecular dynamics simulation. *J. Phys. Chem. B* 108:6603–6610.

61. Mahoney, M. W., and W. L. Jorgensen, 2001. Diffusion constant of the TIP5P model of liquid water. *J. Chem. Phys.* 114:363–366.

62. Mills, R., 1973. Self-diffusion in normal and heavy water in the range $1 - 45^{\circ}$. *J. Phys. Chem.* 77:685–688.

63. Mashl, R. J., H. L. Scott, S. Subramaniam, and E. Jacosson, 2001. Molecular simulation of dioleoylphosphatidylcholine lipid bilayers at different levels of hydration. *Biophys. J.* 81:3005–3015.

64. Pandit, A. A., D. Bostick, and M. L. Berkowitz, 2003. An algorithm to describe molecular rugged surfaces and its application to the study of a water/lipid bilayer interface. *J. Chem. Phys.* 119:2199–2205.

65. Gawrisch, K., D. Ruston, J. Zimmerberg, V. A. Parsegian, R. P. Rand, and N. Fuller, 1992. Membrane dipole potentials, hydration forces, and the ordering of water at membrane surfaces. *Biophys. J.* 61:1213–1223.

66. Pearson, R. H., and I. Pascher, 1979. The molecular structure of lecithin dihydrate. *Nature* 281:499–501.

67. Hauser, H., I. Pascher, R. H. Pearson, and S. Sundell, 1981. Preferred conformation and molecular packing of phosphatidylethanolamine and phosphatidylcholine. *Biochim. Biophys. Acta* 650:21–51.

68. Chandrasekhar, I., M. Kastenholz, R. D. Lins, C. Oostenbrink, L. D. Schuler, D. P. Tieleman, and W. F. van Gunsteren, 2003. A consistent potential energy parameter set for lipids: dipalmitoylphosphatidylcholine as a benchmark of the GROMOS96 45A3 force field. *Europ. Biophys. J.* 32:67–77.

69. Jähnig, F., 1996. What is the surface tension of a lipid bilayer membrane? *Biophys. J.* 71:1348–1349.

70. Liu, Y., and J. F. Nagle, 2004. Diffuse scattering provides material parameters and electron density profiles of biomembranes. *Phys. Rev. E* 69:40901.

Tables

	GAFF		CHARMM27		BERGER			GAFF		CHARMM27		BERGER	
name	type	charge	type	charge	type	charge	name	type	charge	type	charge	type	charge
choline	$\sum$	**1.1**	$\sum$	**1.1**	$\sum$	**1.4**	**acyl chain**	$\sum$	**0.0**	$\sum$	**0.1**	$\sum$	**0.0**
N1	n4	0.02	NTL	-0.60	LNL	-0.50	C2	c3	-0.12	CTL2	-0.08	LP2	0.000
C2	c3	-0.12	CTL5	-0.35	LC3	0.40	H2a/b	hc	0.05	HAL2	0.09		
H2a/b/c	hx	0.11	HL	0.25			C3	c3	-0.02	CTL2	-0.18	LP2	0.000
C3	c3	-0.12	CTL5	-0.35	LC3	0.40	H3a/b	hc	0.02	HAL2	0.09		
H3a/b/c	hx	0.11	HL	0.25			C4	c3	-0.03	CTL2	-0.18	LP2	0.000
C4	c3	-0.12	CTL5	-0.35	LC3	0.40	H4a/b	hc	0.02	HAL2	0.09		
H4a/b/c	hx	0.11	HL	0.25			C5	c3	-0.02	CTL2	-0.18	LP2	0.000
C5	c3	-0.01	CTL2	-0.10	LH2	0.30	H5a/b	hc	0.01	HAL2	0.09		
H5a/b	hx	0.09	HL	0.25			C6	c3	-0.02	CTL2	-0.18	LP2	0.000
C6	c3	0.16	CTL2	-0.08	LC2	0.40	H6a/b	hc	0.01	HAL2	0.09		
H6a/b	h1	0.06	HAL2	0.09			C7	c3	-0.02	CTL2	-0.18	LP2	0.000
							H7a/b	hc	0.02	HAL2	0.09		
phosphate	$\sum$	**-1.28**	$\sum$	**-1.2**	$\sum$	**-1.4**	C8	c3	0.04	CTL2	-0.18	LP2	0.000
O7	os	-0.42	OSL	-0.57	LOS	-0.80	H8a/b	hc	0.03	HAL2	0.09		
P8	p5	1.12	PL	1.5	LP	1.70	C9	c2	-0.25	CEL1	-0.15	LH1	0.000
O9	o	-0.78	O2L	-0.78	LOM	-0.80	H9	ha	0.13	HEL1	0.15		
O10	o	-0.78	O2L	-0.78	LOM	-0.80	C10	c2	-0.24	CEL1	-0.15	LH1	0.000
O11	os	-0.42	OSL	-0.57	LOS	-0.70	H10	ha	0.13	HEL1	0.15		
							C11	c3	0.02	CTL2	-0.18	LP2	0.000
glyercol	$\sum$	**-0.1**	$\sum$	**-0.32**	$\sum$	**-0.2**	H11a/b	hc	0.03	HAL2	0.09		
C12	c3	0.06	CTL2	-0.08	LC2	0.40	C12	c3	-0.01	CTL2	-0.18	LP2	0.000
H12a	h1	0.08	HAL2	0.09			H12a/b	hc	0.01	HAL2	0.09		
H12b	h1	0.08	HAL2	0.09			C13	c3	-0.00	CTL2	-0.18	LP2	0.000
C13	c3	0.14	CTL1	0.04	LH1	0.30	H13a/b	hc	0.00	HAL2	0.09		
H13	h1	0.13	HAL1	0.09			C14	c3	-0.00	CTL2	-0.18	LP2	0.000
C14	c3	0.01	CTL2	-0.05	LC2	0.50	H14a/b	hc	0.00	HAL2	0.09		
H14a	h1	0.10	HAL2	0.09			C15	c3	-0.02	CTL2	-0.18	LP2	0.000
H14b	h1	0.10	HAL2	0.09			H15a/b	hc	0.01	HAL2	0.09		
O15	os	-0.40	OSL	-0.34	LOS	-0.70	C16	c3	-0.01	CTL2	-0.18	LP2	0.000
O16	os	-0.40	OSL	-0.34	LOS	-0.70	H16a/b	hc	0.01	HAL2	0.09		
							C17	c3	0.02	CTL2	-0.18	LP2	0.000
carbonyl	$\sum$	**0.28**	$\sum$	**0.22**	$\sum$	**0.2**	H17a/b	hc	0.01	HAL2	0.09		
C1a	c	0.71	CL	0.63	LC	0.80	C18	c3	-0.13	CTL3	-0.27	LP3	0.000
O1a	o	-0.57	OBL	-0.52	LO	-0.60	Ha/b/c	hc	0.03	HAL3	0.09		
C1b	c	0.71	CL	0.63	LC	0.70							
O1b	o	-0.57	OBL	-0.52	LO	-0.70							

Table 1: The atom-types and the partial charges of all atoms used in the respective force fields.

system	# lipid	#water	lipid force field	water model	ensemble
A	72	2727	GAFF all-atom	SPC/E	*NPT*
B	72	2727	GAFF all-atom	SPC/E	$NP\gamma T$
C	72	2727	GAFF all-atom	TIP3P	$NP\gamma T$
D	72	2727	CHARMM all-atom	TIP3P	$NP\gamma T$
E	128	4789	BERGER united-atom	SPC	*NPT*

Table 2: Overview of the simulation systems presented in this study.

system	area per lipid (nm^2)	membrane thickness (nm)
exp†	*0.721*	*3.71*
A	0.62 ± 0.01	4.00 ± 0.05
B	0.72 ± 0.01	3.61 ± 0.04
C	0.74 ± 0.03	3.51 ± 0.13
D	0.71 ± 0.01	3.63 ± 0.13
E	0.66 ± 0.01	3.72 ± 0.11

Table 3: Averages and errors of the membrane structural parameters calculated by block averaging (block length 20 ns). The membrane thickness was measured as the distance between the two peaks in the system electron density profiles. Errors in the area per lipid for systems D and E were rounded to 0.01 nm^2. †The experimental values were measured by Liu and Nagle (70) using fully hydrated DOPC bilayers at 30° C.

system	most probable orientation (°)	width at half maximum (°)	$M \pm \sigma$ (Debye)	M_z (Debye)
A	59	$79 \left(^{+46}_{-33}\right)$	23.2 ± 3.8	4.3
B	67	$74 \left(^{+36}_{-38}\right)$	23.2 ± 2.8	4.0
C	69	$82 \left(^{+39}_{-43}\right)$	23.3 ± 2.7	3.5
D	73	$62 \left(^{+32}_{-30}\right)$	23.7 ± 3.2	2.1
E	86	$88 \left(^{+32}_{-56}\right)$	27.1 ± 3.8	8.1

Table 4: Distribution of lipid headgroup orientations computed as the angle between the vector connecting the phosphorus and the nitrogen atoms and the bilayer normal. Both the maximum of the distribution – the most probable orientation – as well as its width are given. The last two columns give the most probable total dipole moment of the individual lipids in the respective force fields ($\pm$ the width of a fitted Gaussian distribution) as well as the average of the dipole moment along the bilayer normal (z-direction).

system	water diffusion ($\times 10^{-5} cm^2 s^{-1}$)	lipid diffusion ($\times 10^{-8} cm^2 s^{-1}$)
exp		13.7†
A	2.27 ± 0.03	1.79 ± 0.51
B	2.07 ± 0.03	3.13 ± 0.94
C	4.31 ± 0.08	5.71 ± 1.06
D	4.60 ± 0.08	11.76 ± 3.39
E	3.63 ± 0.02	5.52 ± 1.00

Table 5: The calculated mean lateral diffusion coefficient for water molecules and for DOPC molecules. For water diffusion, the average was calculated from all water molecules in the system regardless of the distance to bilayer. For lipid diffusion, the long-range diffusion coefficients are shown here while the short-range diffusions are depicted in Figure 6. The experimental lipid diffusion coefficient is taken from pulsed field gradient NMR experiments on oriented bilayers at 308 K (57).

Figure Legends

Figure 1.

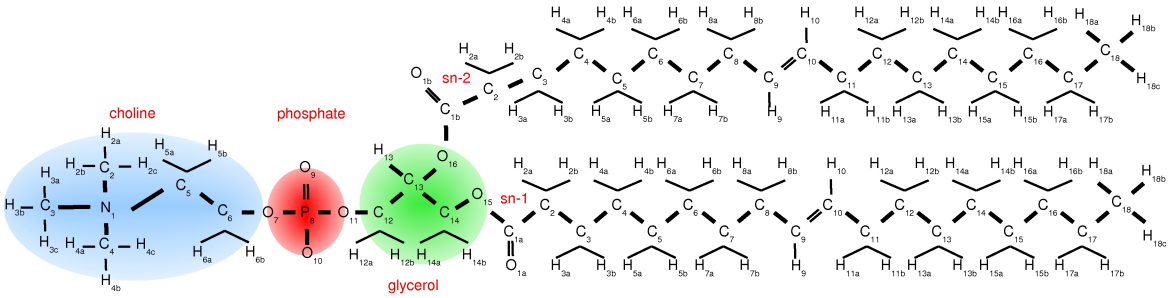

Figure 1

Schematic drawing of the DOPC lipid and the naming convention used in this manuscript.

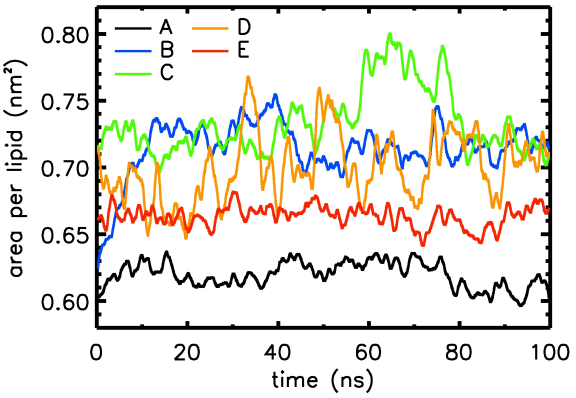

Figure 2

Figure 2.

Area per lipid for the five investigated systems in 100 ns simulation time smoothed by a sliding window of 1 ns length. Larger fluctuations were observed for systems applying surface tension (B, C, and D) as compared to those using semi-isotropic pressure coupling (A and E). Note that the experimental area per lipid for DOPC was measured to be 0.721 nm^2 at 30° C (70).

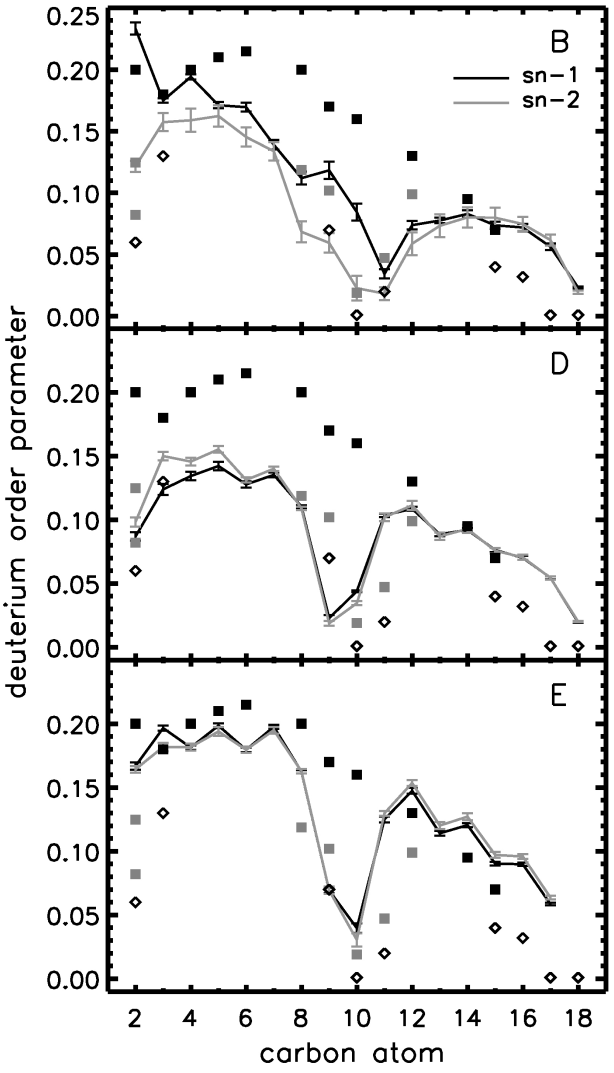

Figure 3

Figure 3.

Deuterium order parameters, $|S_{CD}|$, for the two acyl chains of DOPC lipids analyzed for systems B, D, and E. Error bars indicate the errors of the means from block averaging (blocks of 20 ns length). Experimental values are given for the POPC *sn*-1 (*black squares*) and *sn*-2 chain (*gray squares*) at 27°C (48), and for DOPC *sn*-2 at 37°C (50) ($\diamond$ symbols). Note that the double-bonded carbon atoms are at positions 9 and 10.

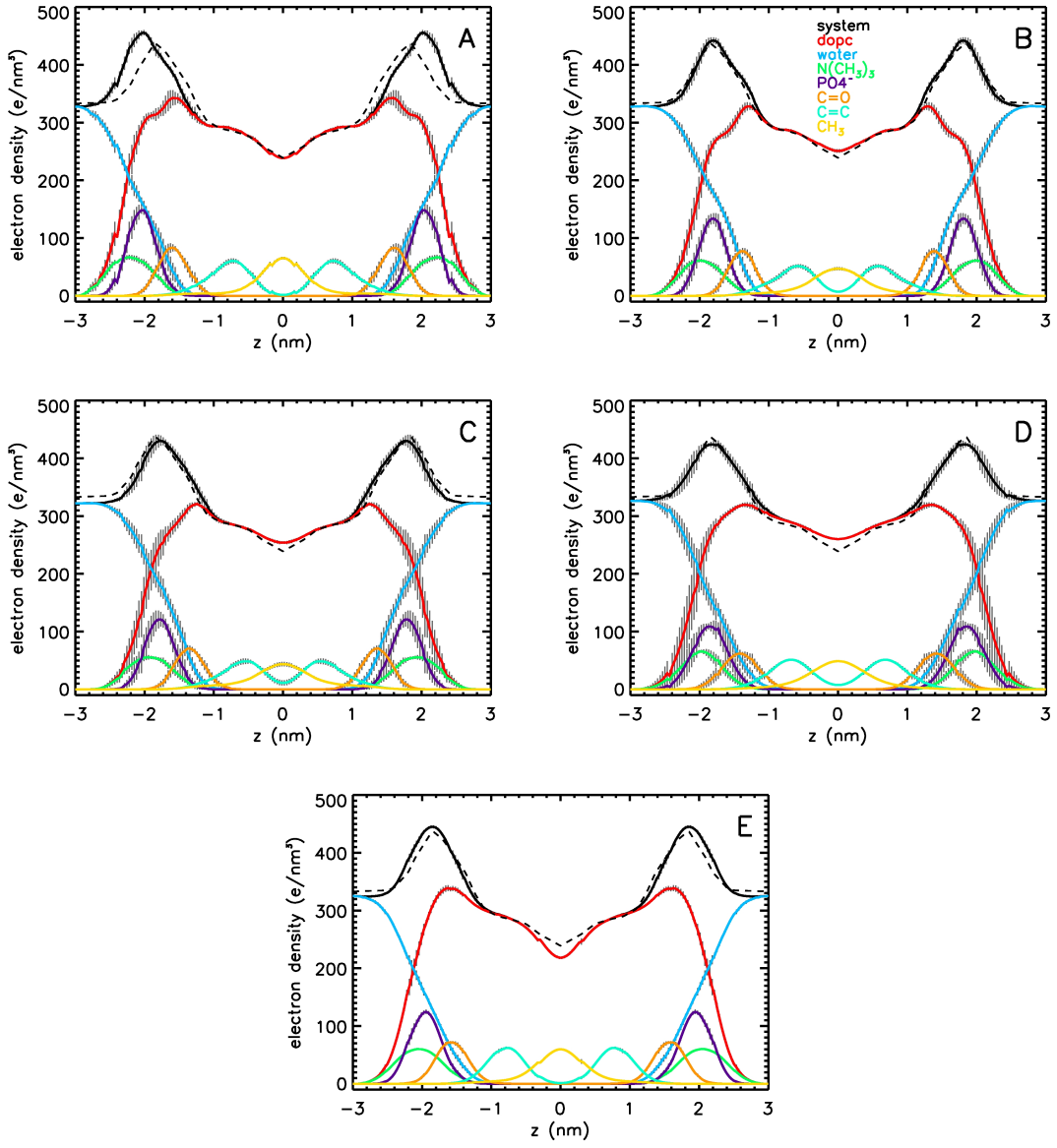

Figure 4

Figure 4.

The (symmetrized) electron density profiles of the overall and individual chemical components of all simulation systems. The profiles are centered at the core of the bilayer, and the standard errors (as shown here in *gray* lines) are calculated by dividing the trajectories into blocks of 20 ns length. The profile was computed by placing the appropriate number of electrons at the center of atomic nuclei binning along the direction of the membrane normal (bin width 0.3 Å). The experimental density profile (70) is shown as a *dashed* line.

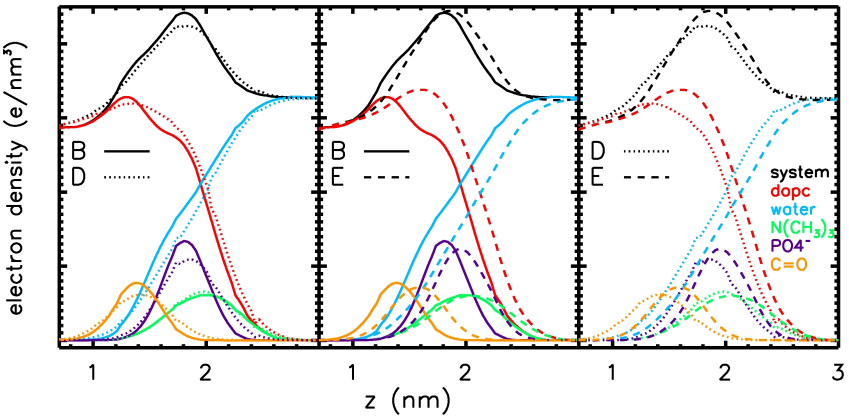

Figure 5

Figure 5.

Comparison of the electron density profiles at the membrane-water interface (centered on the lipid bilayer) for force field combinations GAFF-SPC/E, CHARMM27-TIP3P and Berger-SPC (systems B, D and E).

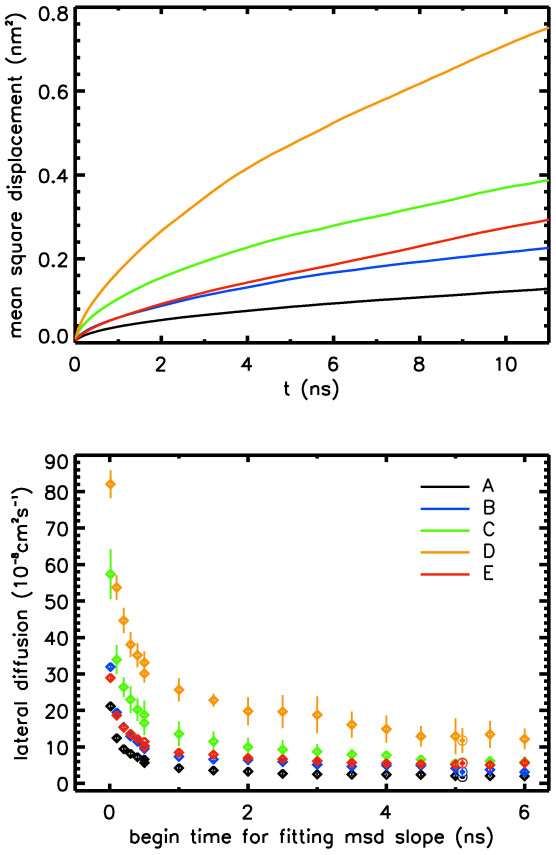

Figure 6

Figure 6.

Lipid diffusion coefficients calculated for different time length of the simulations by block averaging: The trajectory was divided into 20 ns pieces and the mean square displacement (msd, upper panel) was calculated separately for each block. Diffusion coefficients (lower panel) computed for different time ranges were obtained by fitting different time windows of the msd curve. For the short-range diffusion (colored $\diamond$ symbols), shorter time windows of 100 ps (fit starts between 10 and 500 ps) and 500 ps (fit starts between 500 ps and 6 ns) were used. For the long-range diffusion (colored $\odot$ symbols) fitting was done on the linear segment of the msd curve between 5 ns and 10 ns.

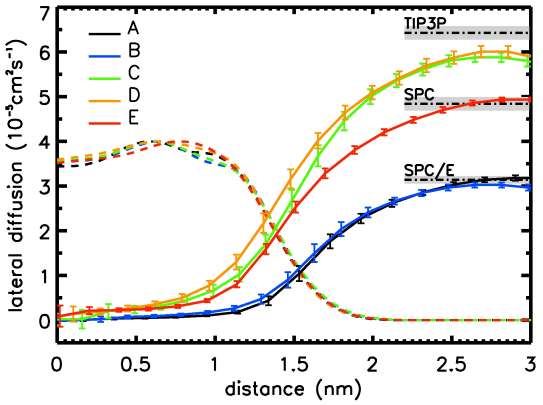

Figure 7

Figure 7.

The lateral diffusion coefficients of water molecules (*solid* lines) at the membrane-water interface. The *dashed* lines mark the normalized DOPC electron density profiles (superimposed at the descending slope) to indicate the location of the bilayer. The respective values for bulk water diffusion are shown as *dashed-dotted* lines (errors in *gray* shading). All diffusion coefficients (and standard errors) were measured by fitting the slope between 2 – 200 ps of the mean square displacement curves, using block averaging of length 5 ns.

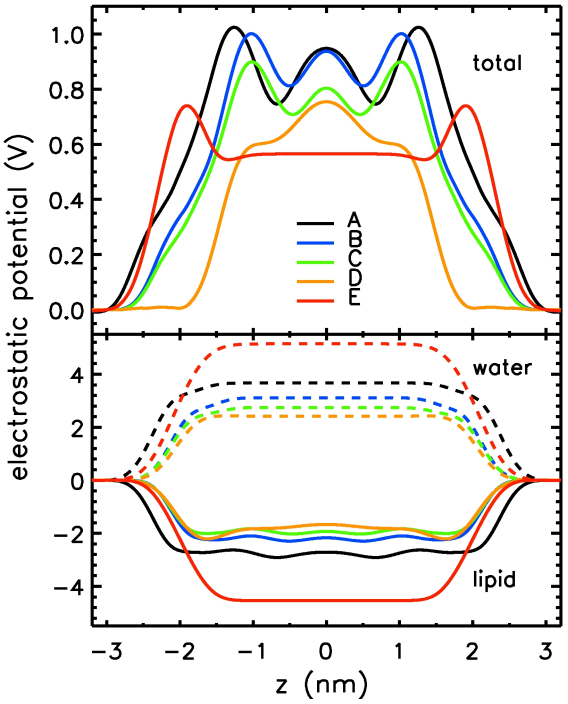

Figure 8

Figure 8.

Total electrostatic potential (upper panel) and contributions (lower panel) due to the lipid dipoles (*solid* lines) and due to water dipole orientation (*dashed* lines) at the membrane/water interface across the DOPC bilayer (symmetrized). The potential was averaged over the final 80 ns of the simulation.

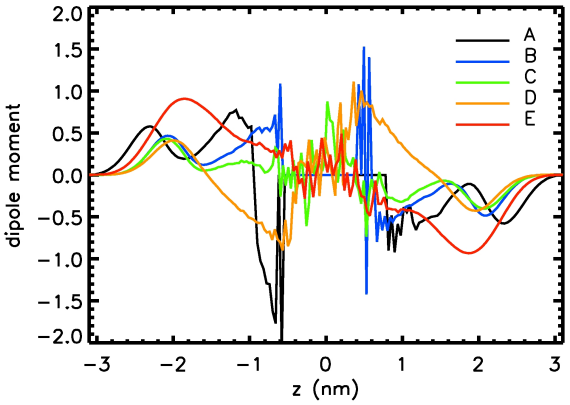

Figure 9

Figure 9.

Average water dipole moment along the membrane normal. The large fluctuations inside the hydrophobic core of the lipid bilayer are due to individual water molecules spontaneously permeating the membrane.